NANO LETTERS
Cite This: Nano Lett. 2019, 19, 482−487
Letter
pubs.acs.org/NanoLett

Temperature-Dependent Transport in Ultrathin Black Phosphorus Field-Effect Transistors

Xiaodong Yan,[†] Han Wang,*[,†] and Ivan Sanchez Esqueda*[,‡]

[†]Ming Hsieh Department of Electrical Engineering, University of Southern California, Los Angeles, California 90089, United States
[‡]Information Sciences Institute, University of Southern California, Marina del Rey, California 90292, United States

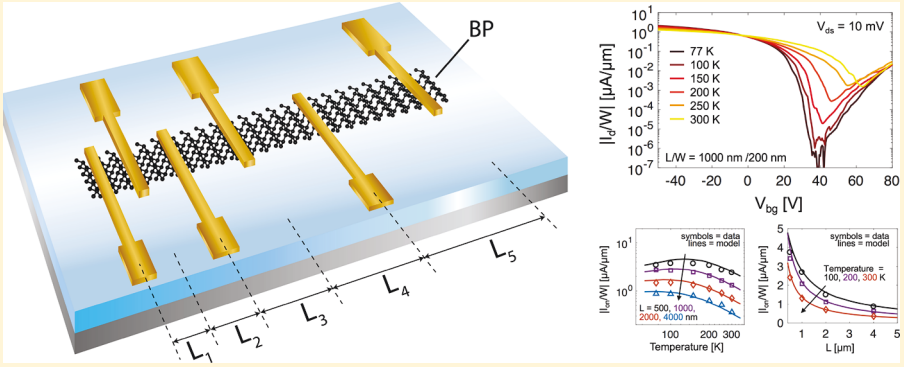

ABSTRACT: We studied the temperature-dependent transport properties of ultrathin black phosphorus (BP). We present measurements of BP Schottky barrier (SB) metal-oxide-semiconductor field-effect-transistors (MOSFETs) with various channel lengths, constructed from a single BP sample with nanoscale uniformity in thickness and width. The electrical characterization reveals a reversal in the temperature dependence of drain current as a function of gate voltage. This reversal indicates a transition in the charge conduction limiting mechanisms as the device is swept from the off-state into the on-state. In the off-state, charge transport is limited by thermionic emission over the energy barriers at the source/drain SB contacts, and drain current increases with temperature. In the on-state, carriers can easily tunnel across the SB at the contacts, and charge transport is limited by scattering in the channel. As a result, drain current decreases with temperature in the on-state, as scattering increases with temperature. Using Landauer transport theory, we derive a closed-form expression for thermionic emission current in SB-MOSFETs with two-dimensional channels. We use this expression to extract the SB height at metal contact interface with BP and demonstrate the impact of scattering on the extraction. We then use a comprehensive BP SB-MOSFET model to analyze on-state current as a function of temperature and demonstrate the effects of charged impurity and phonon scattering on the transport properties of BP through extractions of mobility at fixed carrier density.

KEYWORDS: *Black phosphorus, MOSFET, transistor, transport, two-dimensional, 2D materials*

Since the rediscovery of black phosphorus (BP) as a promising two-dimensional (2-D) layered material for electronic and optoelectronic applications,[1−4] several studies have explored the transport properties of BP[5−8] and the electrical characteristics of nanoscale devices with BP channels.[9−12] The operation of Schottky barrier metal-oxide-semiconductor field-effect-transistors (SB-MOSFETS) is of significant technological importance for electronic applications with 2-D channel materials and metal source/drain contacts.[1,13−16] In 2013, Das et al. utilized conventional thermionic emission theory to extract the SB height at the interface between thin MoS_2 flakes and metal contacts and demonstrate the impact of metal work function on the transport properties of SB MOSFETs with 2-D channels.[17] Later, Penumatcha et al. presented an analytical model based on Landauer's formalism to analyze the transport properties of BP SB-MOSFETs.[15] This model neglected scattering in the channel but was successfully applied to fit experimental data in the device off-state region of operation and extract SB heights as a function of BP channel thickness. Recently, Esqueda et al. presented an improved analytical SB-MOSFET model that incorporates channel scattering as well as the effects of interface traps and quantum capacitance through a self-consistent calculation of the channel potential.[16] This model was used to analyze transport properties in ultrathin BP devices with and without hexagonal boron nitride (hBN) insulation and demonstrate improvements in mobility due to screening of charged-impurity- and roughness-induced phonon scattering.

In this work, we present new analysis of transport in BP, by measuring the temperature- and channel-length (L)-dependent electrical characteristics of SB MOSFETs with ultrathin BP channels. Based on this characterization, we demonstrate the

Received: October 25, 2018
Revised: November 30, 2018
Published: December 5, 2018

DOI: 10.1021/acs.nanolett.8b04308
Nano Lett. 2019, 19, 482−487

importance of scattering effects on analyzing transport across SB at the interface between metal contacts and 2-D channel materials (previously neglected). We also derive a more valid expression for thermionic emission current in SB-MOSFETs using the Landauer formalism, which should replace the conventional expression used by Das et al.[17] when extracting SB height in nanoscale devices with 2-D channels. We apply this new expression to extract the SB height at the metal/channel interface of BP devices. We also demonstrate the impact of channel scattering on the extraction of SB height by applying this technique on devices with increasing channel lengths. Then, using the improved model of Esqueda et al.,[16] we analyze BP SB-MOSFET on-state current as a function of temperature. We use model fits to the temperature-dependent data to extract field-effect mobility at a fixed carrier density, and demonstrate the contribution of charged impurity and phonon scattering on the transport properties of BP SB-MOSFETs. The modeling approach accounts for device parameters and material properties (e.g., dimensionality, density-of-states, quantum capacitance, etc.) as well as extrinsic effects (e.g., interface states and charge trapping).

EXPERIMENTAL RESULTS

For this work, we fabricated BP SB-MOSFETs through the mechanical exfoliation and dry transfer of BP onto a 300 nm SiO_2/Si substrate. A narrow BP flake with rectangular shape and with uniform thickness was carefully selected through visual inspection of the optical contrast on BP flakes on the substrate. Exfoliation and transfer were performed in an ultrahigh purity 99.999% argon-filled glovebox (MBraun Inc.) with low oxygen and water concentration (i.e., <0.1 ppm), to ensure the quality of the BP samples. The samples were then coated with PMMA (poly(methyl methacrylate)) resist and contact regions with increasing separating distance were patterned using a Raith 20 kV electron beam lithography (EBL) system. Cr/Au (5/30 nm) contacts were formed through thermal evaporation using a Kurt J. Lesker Nano 36 system and lift-off process. Figure 1(a) is a schematic of the sample used in this study. The sample was loaded into a vacuum probe station (<5×10^{-6} Torr) and annealed at 350 K for 1 h. Using the Si substrate as a common back-gate, we measured the electrical characteristics of SB-MOSFETs with increasing channel lengths labeled in Figure 1(a) as L_1 through L_5. The electrical characterization was performed at various temperatures from room temperature to 77 K. After the electrical characterization, atomic force microscopy (AFM) was used to measure the thickness, surface roughness, and geometry of the BP channel in the sample devices. Figure 1(b) is the AFM image of the sample, and Figure 1(c) is a plot of the height profile of the BP flake extracted from AFM measurements across the center of the channel region for the various SB-MOSFETs. The AFM measurements reveal the nanoscale uniformity of the BP flake thickness and width. The channel width (W) for all SB MOSFETs is ~200 nm (extracted at the midpoint of the BP flake thickness). The thickness is approximately 13 nm for SB-MOSFET with L_1 = 250 nm, and approximately 9 nm for all other devices.

Figure 2(a) plots measurements of drain current (I_d) per unit width (W) as a function back-gate voltage (V_{bg}) from the BP SB-MOSFETs with L = 1000 nm, for all temperatures (77, 100, 150, 200, 250, and 300 K). These are dual gate sweeps that reveal gate hysteresis in the I_d–V_{bg} characteristics. With increasing temperature, the effect is enhanced, indicating a

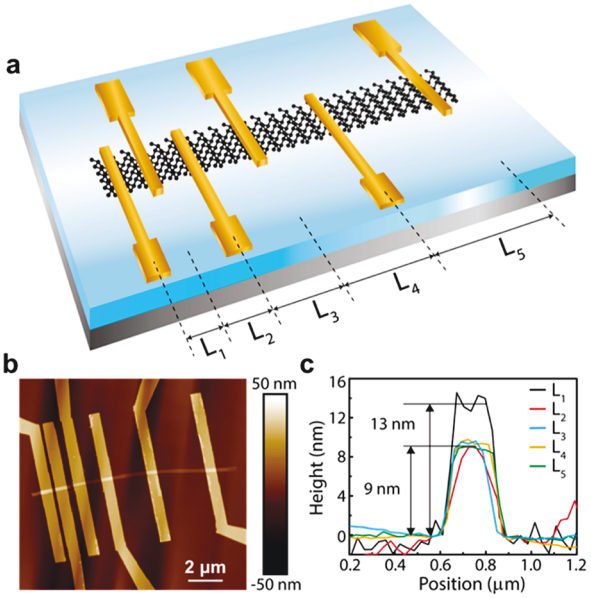

Figure 1. (a) 3-D schematic of the black phosphorus device with channel lengths L_1 = 250 nm, L_2 = 500 nm, L_3 = 1000 nm, L_4 = 2000 nm, L_5 = 4000 nm. (b) AFM image of BP device. (c) AFM height profile indicating a thickness of ~13 nm for device with L_1 = 250 nm, and ~9 nm for all other devices. Channel width is approximately 200 nm for all devices (extracted at midpoint).

wider contribution of traps to the charge trapping effects that cause gate hysteresis. With increasing temperature we also observe a reduction of the on/off ratio, due to a wider range of energies contributing to carrier conduction in the channel. This results in a larger overlap of the hole and electron branches, effectively raising I_d at the minimum value which corresponds to the gate voltage at which the branches intersect. For easier visualization, in Figure 2(b) we plot the I_d–V_{bg} characteristics from only the negative gate sweep direction (positive to negative V_{bg}). The measurements in Figure 2(b) reveal that the gate voltage at the minimum I_d (i.e., V_{min}) shifts to larger positive values with increasing temperature, indicating a net negative change on the charge contribution from traps. This can be attributed to an increased occupancy of acceptor-like traps, as more electrons can be captured at higher temperatures under the initial condition of the sweep with a large positive V_{bg} bias. Figure 2(c) plots the change in V_{min} (and the corresponding change in density of charged acceptor-like traps) as a function of the temperature. In Figure 2(d) we plot I_d as a function of $V_{bg} - V_{min}$, to effectively offset the electrostatic effect (voltage shift) due to traps contributing to gate hysteresis. The resulting I_d vs $V_{bg} - V_{min}$ plot indicates that current flow increases with temperature in the off-state, and decreases with temperature in the on-state. In Figure 2(e) we plot the on-state drain current (I_{on}) at a fixed bias of $V_{bg} - V_{min} = -80$ V, which corresponds to an approximate hole density of $p_s \approx -(C_{ox}/q)(V_{bg} - V_{min}) = 5 \times 10^{12}$ cm^{-2}, as a function of temperature for SB-MOSFETs with increasing channel lengths. The error bars indicate ±20% error tolerance in the extraction of I_{on} resulting from uncertainty in W (determined from AFM measurements), and uncertainty in V_{min} extracted from the I–V characteristics. We note that the largest uncertainty in V_{min} was determined to be approximately ±2.5 V at 77 K (i.e., due to noise at low I_d), and has only a

DOI: 10.1021/acs.nanolett.8b04308
Nano Lett. 2019, 19, 482–487

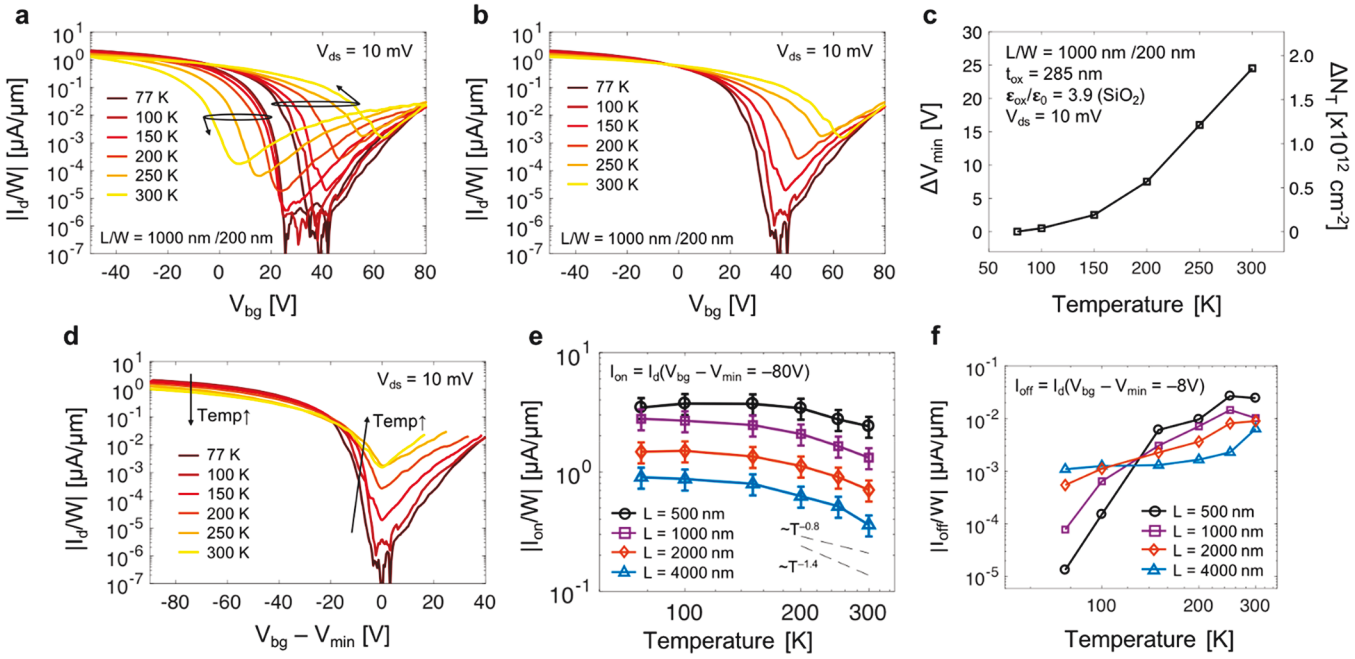

Figure 2. (a) Dual gate sweeps of transfer characteristics (I_d–V_{bg}) for the device with L/W = 1000/200 nm at various temperatures. (b) Negative gate sweep of I_d–V_{bg} for the device with L = 1000 nm. (c) Temperature dependence of change in V_{min} and density of charged traps N_T. (d) Negative gate sweep of I_d–V_{bg} with gate voltage axis offset by V_{min}. (e) Temperature dependence of I_{on} at a fixed bias of $V_{bg} - V_{min}$= −80 V for devices with increasing channel lengths. (f) Temperature dependence of I_{off} at a fixed bias of $V_{bg} - V_{min}$= −8 V for devices with increasing channel lengths.

small effect on extractions of I_{on}. The 20% tolerance safely accounts for miscalculation in W from AFM measurements.

The results in Figure 2(e) show I_{on} decreasing with L, and a transition from an initially temperature-independent current to a $T^{-\gamma}$ dependence with γ around 0.8 and 1.4. These observations are consistent with scattering in the BP channel because I_{on} is proportional to λ/L, where λ is the carrier backscattering mean free path which captures the scattering mechanisms in the channel (and their temperature dependence).[18−20] We will show that the transition in the temperature-dependence of I_{on} results from a transition of the dominant scattering mechanisms from charged-impurity to phonon scattering.

In Figure 2(f) we plot the off-state drain current (I_{off}) as a function of temperature for BP SB-MOSFETs with increasing channel length at a fixed bias of $V_{bg} - V_{min}$ = −8 V. In the off-state, current flow is limited by the Schottky barrier at the interface between the source/drain metal contacts and the BP channel, and increases with temperature due to thermionic emission of carriers over the barrier. With increasing L, the role of scattering becomes more significant and can become the limiting factor toward lower $V_{bg} - V_{min}$ bias (less negative bias), reversing the temperature-dependence as of I_{off}. As a result, the rate at which I_{off} increases with temperature is significantly reduced with L as shown in Figure 2(f). In the following analysis we demonstrate how this affects the commonly used techniques for extracting SB heights.

SB Analysis. As indicated by Das et al.,[17] the metal/semiconductor contact interface is a major performance-limiting factor for devices constructed with low-dimensional materials. Thus, understanding its impact on carrier transport is important for analyzing SB-MOSFETs with 2-D channels. SB heights can be extracted based on the temperature-dependent study of thermionic emission and thermally assisted tunneling. Earlier work used an equation for thermionic emission current in bulk devices expressed as $I_d = AT^2\exp[(q\Phi_B)/(k_BT)]\{1-\exp[-(qV_{ds})/(k_BT)]\}$.[17] It is useful to have a closed form expression for current due to thermionic emission over the barrier at the interface between metals and 2-D channels (see Figure 3(a) for thermionic emission of holes). A derivation based on Landauer's formalism is presented in the Appendix, resulting in the (hole) current expressed as

$$I = V_{ds}WK\sqrt{k_BT}\,e^{-\Phi_B/k_BT} \quad (1)$$

where $K = (q^2/h)(g_v/\hbar)\sqrt{2m_h^*/\pi}$. As illustrated by the band diagram in Figure 3(a), when the device is biased in the off-state, the barrier height (Φ_B) is determined by the energy difference between the top of the valence band in the channel, and the Fermi-level at the contact. At "flat-band" Φ_B corresponds to the SB height for holes ($\Phi_{SB,p}$). As plotted in Figure 3(b), holes injected from the contact follow the Fermi–Dirac distribution. The probability of holes occupying energy levels available for conduction in the valence band (i.e., above the barrier) increases exponentially with temperature.[21] Thus, thermionic current increases exponentially with temperature. The barrier height can be extracted experimentally from the slope of $\log[I_{off}/(V_{ds}WK\sqrt{k_BT})]$ plotted vs $1/T$ (Figure 3(c)). In Figure 3(d) we plot the extracted barrier height as a function of $V_{bg} - V_{min}$ for SB-MOSFETs with L = 500, 1000, 2000, and 4000 nm (symbols). Above flat-band, the barrier at the interface no longer changes, but the extracted Φ_B continues to drop, although at a reduced rate, due to the increasing contribution of thermally assisted tunneling. The flat-band condition is determined from the linear dependence deviation of Φ_B as a function of $V_{bg} - V_{min}$. Figure 3(e) plots the extracted SB height (Φ_{SB}) as a function of L. The extracted

DOI: 10.1021/acs.nanolett.8b04308
Nano Lett. 2019, 19, 482−487

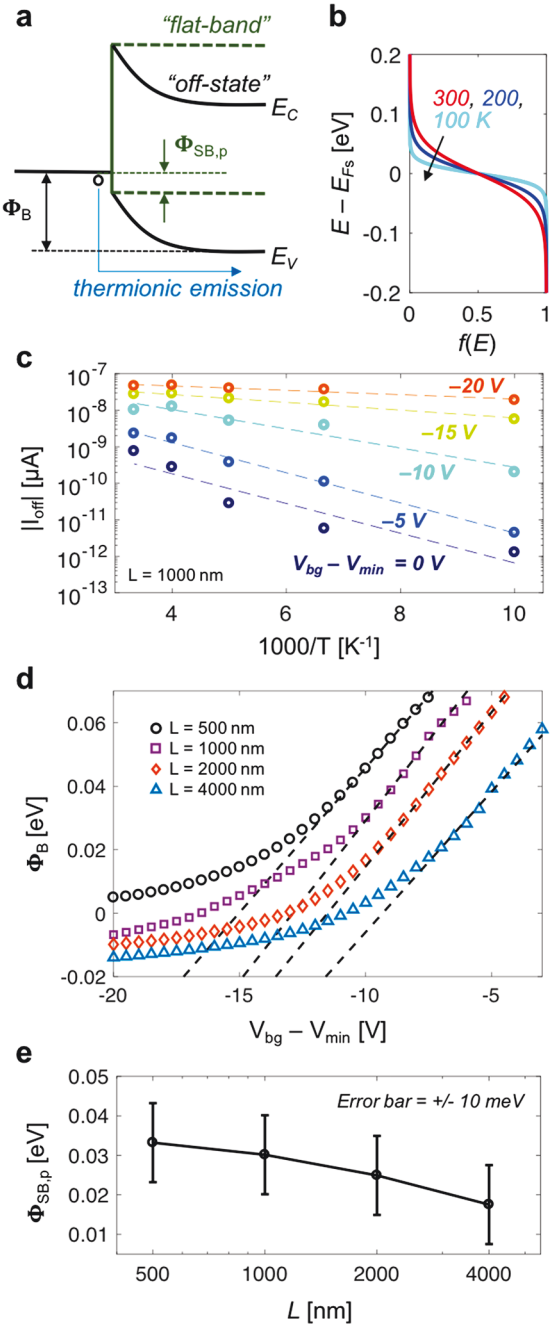

Figure 3. (a) Band diagram shows barrier for holes. (b) Fermi−Dirac distributions of holes injected from the contact at different temperatures. (c) Arrhenius-type plot of I_{off} vs $1/T$ at different $V_{bg} - V_{min}$. (d) Extracted barrier heights for devices with increasing channel lengths. Inset plot shows SB heights extracted for devices with various channel lengths.

value drops down from ∼30 meV for L = 500 nm, to ∼15 meV for L = 4000 nm, due to the more significant contribution of scattering on the temperature-dependence of I_{off}. If we extrapolate the extracted SB height back to small L, where scattering is negligible, we obtain a Φ_{SB} ∼35 meV. Such small energy barrier for holes is consistent with the dominant p-type conduction that is achieved on the BP SB-MOSFETs used in this work. The error bars in Figure 3(e) indicate a ±10 meV uncertainty in the extraction of Φ_{SB} that may result due to discrepancies in the fits of I_{off} vs T resulting from miscalculations in extractions of V_{min}.

Scattering Effects. We measured the temperature- and channel-length-dependence of I_{on} in SB-MOSFETs, indicating a transition of the dominant scattering mechanism as a function of temperature. We now analyze the transport properties of thin and narrow BP channels by fitting these experimental results with our previously demonstrated model for SB-MOSFETs.[16] Shown in Figure 4(a) are model fits to the experimental I_d vs V_{bg} characteristics for the device with L = 2000 nm and for increasing temperatures. For the model calculations we have used the SB height for holes extracted experimentally (i.e., $\Phi_{SB,p}$ = 0.035 eV), and $\Phi_{SB,n}$ = 0.265 eV for electron, resulting in a bandgap of $E_G = \Phi_{SB,n} + \Phi_{SB,p}$ = 0.3 eV. The fit to the experimental results required adjusting the density and energy distribution of interface traps (acceptor- and donor-like traps, $D_{it,a}$ and $D_{it,d}$), used in a self-consistent calculation of channel potential as given by $V_C = (V_g - V_{FB})[C_{ox}/(C_{ox} + C_q)]$.[22−24] $C_q(V_C)$ and $V_{FB}(V_C)$ are the quantum capacitance and flat-band voltage, and are a function of V_C. V_{FB} accounts for the work-function difference between the gate and channel, as well as the charge contribution from ionized (i.e., charged) interface traps. We use simple Gaussian distributions for both $D_{it,a}(E)$ and $D_{it,d}(E)$, plotted in Figure 4(b), that result in reasonable agreement with the experimental I−V characteristics, and help capture the observed trends as a function of L and temperature. In these calculations, the channel potential represents the amount of band bending in the channel with respect to the Fermi levels in the source/drain contacts. Thus, the modeling approach self-consistently accounts for the bias-dependent impact of trap occupancy on band bending as a function of V_g.

The mean free path $\lambda(E)$, is modeled by incorporating charged-impurity (λ_{ci}) and phonon (λ_{ph}) scattering components as $1/\lambda(E) = 1/\lambda_{ci}(E) + 1/\lambda_{ph}(E)$.[18,19] Each component is described by a power-law function of energy where $\lambda(E) = \lambda_0[(E_V - E)/(k_BT)]^r$, where $r = {}^3/_2$ for charged impurity scattering and $r = {}^1/_2$ for phonon scattering.[18,19,25−27] For charged-impurity scattering λ_0 depends on the density of charged traps (N_{it}) and is modeled as $\lambda_{0ci} = N_{0ci}/N_{it}$. The larger temperature dependence of I_{on} for T > ∼150 K is captured by the phonon scattering component using $\lambda_{0ph} = N_{0ph}/T^n$.[18,19] N_{0ci}, N_{0ph}, and n are the model fitting parameters used to capture the temperature and channel length dependence of I_{on} plotted respectively in Figures 4(c) and 4(d). For these model fits we have used $N_{0ci} = 8 \times 10^{13}$ cm^{-2}, $N_{0ph} = 3.8 \times 10^7$, and n = 2.4. The model calculations result in good fits with experimental data for I_{on} as a function of L and temperature. A better understanding of the scattering mechanisms and their temperature dependence can be obtained by calculating hole mobility as a function of temperature at a fixed carrier concentration (p_s). These calculations are shown in Figure 4(e) for $p_s = 10^{12}$ cm^{-2}, using the same model parameters used to fit I_{on}. The results in Figure 4(e) indicate a mobility limited by charged impurity scattering with negligible temperature dependence below ∼T = 100 K. For temperatures between 100 K and room temperature, calculations indicate a transition to a phonon-scattering limited mobility with a large temperature dependence approximating a power-law $T^{-\gamma}$ dependence. This large temperature dependence is consistent with previous studies,[9] and has been attributed to a large contribution of acoustic phonons.

DOI: 10.1021/acs.nanolett.8b04308
Nano Lett. 2019, 19, 482−487

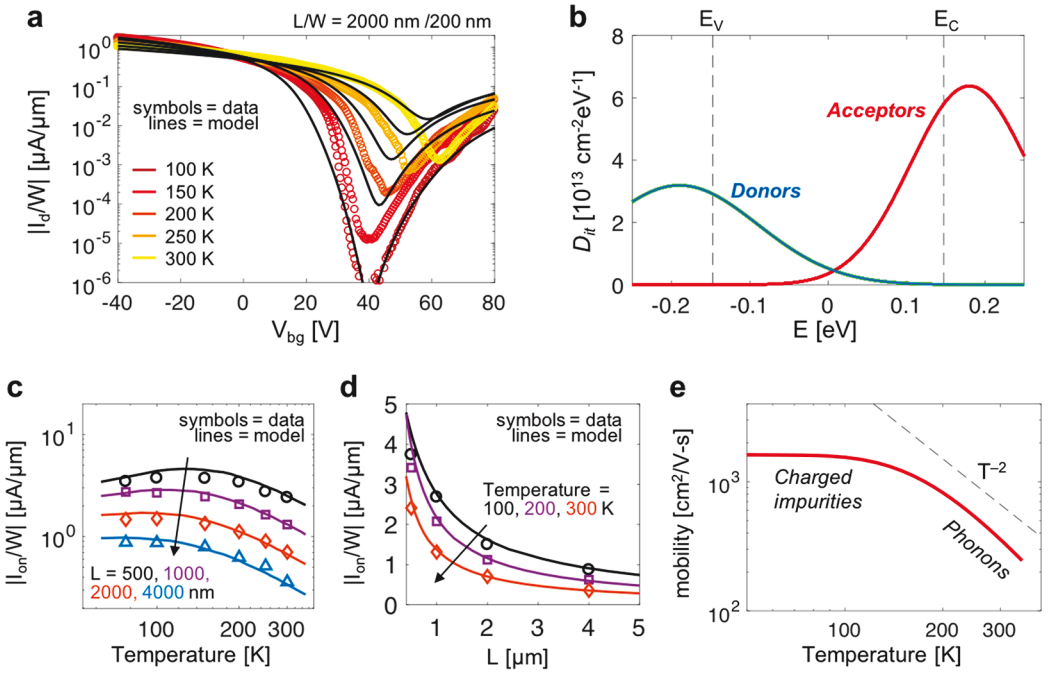

Figure 4. (a) Fits of model calculations to the experimental I_d-V_{bg} for the device with L = 2000 nm. (b) D_{it} for donors and acceptors. (c) Model calculation and experimental extractions of temperature dependence of I_{on} for devices with increasing channel lengths. (d) Model calculation and experimental extractions of channel lengths dependence of I_{on} at increasing temperatures. (e) Temperature dependence of extracted hole mobility in BP SB−MOSFETs.

In conclusion, we present new analysis of transport in ultrathin BP SB-MOSFETs with various channel lengths using temperature-dependent measurements from 300 to 77 K. From a device physics point-of-view, these results confirm our general understanding of SB-MOSFETs with 2-D channels and provide new observations that indicate the impact of scattering on transport in BP devices as a function of channel length and the effects on SB height analysis/extraction techniques. Our measurements show that I_d increases with temperature in the off-state but decreases with temperature in the on-state. This is explained by the charge conduction limiting mechanism transitioning from thermionic emission of charges over the SB at the interface of contacts/channel in the off-state to channel carrier scattering in the on-state. Based on Landauer's formalism, we present a generalized technique for analyzing thermionic emission current in SB-MOSFETs with 2-D materials. We derive a closed-form expression for BP SB-MOSFETs and apply it to extract the SB height at the source/drain contacts using standard methods based on the slope of the off-state current vs temperature. Our results indicate the impact of scattering, observed as a gradual decrease of extracted SB height with increasing channel length. This is attributed to a more significant role of channel scattering, compared to thermionic emission at the SB, in devices with longer channels.

The temperature dependence of hole mobility is extracted from model fits to the on-state current. Our results indicate a transition of the dominant scattering mechanism from charged-impurity to phonon scattering, as observed from a transition in the temperature dependence of mobility. The characterization and modeling techniques presented in this work were used to investigate the operation and transport properties of SB-MOSFETs with 2-D channel materials and allow consideration of intrinsic material and device properties (e.g., density of states, channel material bandgap, contact work functions, etc.) as well as extrinsic effects (e.g., interface trap density and distribution). These considerations eliminate discrepancies that may arise due to the electrostatic effect of charged traps and enable true calculations of mobility as a function of temperature at fixed carrier densities. The results show that mobility can exceed 1000 $cm^2/V{\cdot}s$ and remain fairly independent of temperature below 100 K. With temperature increasing above 100 K, hole mobility is reduced following a power-law dependence to about 300 $cm^2/V{\cdot}s$ at room temperature.

APPENDIX

The derivation starts with the Landauer equation for hole conduction in the valence band of BP SB-MOSFETs given by

$$I = \frac{2q}{h}\int_{-\infty}^{E_V} T(E)M(E)[f_s - f_d]\mathrm{d}E \tag{2}$$

where q is the electronic charge, h is Planck's constant, $T(E)$ and $M(E)$ are the transmission coefficient and density of modes, respectively, and f_s and f_d are the Fermi functions at the source and drain, respectively. For small V_{ds} we can approximate $f_s - f_d \approx -qV_{ds}(\partial f_0/\partial E)$, and under the Boltzmann approximation $\partial f_0/\partial E \approx (1/k_BT)\exp[(E - E_{F0})/(k_BT)]$. In the off-state, $T(E) = 0$ for $E > E_V$ and 1 for $E < E_V$ (ignoring scattering). Because the limits of integration are for $E < E_V$, we can simply set $T(E) = 1$. For 2-D BP, the density of modes is given by $M(E) = W(g_v/\pi\hbar)\sqrt{2m_h^*(E_V - E)}$ where g_v is the valley degeneracy and m_h^* is the hole effective mass in the valence band. Overall we have

DOI: 10.1021/acs.nanolett.8b04308
Nano Lett. 2019, 19, 482−487

$$I = V_{ds} W \frac{2q^2}{h} \frac{g_v}{\pi\hbar} \frac{\sqrt{2m_h^*}}{k_B T} \int_{-\infty}^{E_V} \sqrt{(E_V - E)}\, e^{\frac{-(E_{F0}-E)}{k_B T}} dE \quad (3)$$

By expressing the SB height as $\Phi_{SB} = E_{F0} - E_V$ (see Figure 3(a)) and changing variable $x = \sqrt{(E_V - E)}$ we obtain

$$I = V_{ds} W \frac{2q^2}{h} \frac{g_v}{\pi\hbar} \frac{\sqrt{2m_h^*}}{k_B T} e^{\frac{-\Phi_{SB}}{k_B T}} 2\int_0^{\infty} x^2 e^{-x^2/k_B T} dx \quad (4)$$

Finally, using $\int_0^{\infty} x^2 e^{-ax^2} dx = \frac{1}{4}\sqrt{\frac{\pi}{a^3}}$ we obtain

$$I = V_{ds} W K \sqrt{k_B T}\, e^{-\Phi_{SB}/k_B T} \quad (5)$$

where $K = \frac{q^2}{h}\frac{g_v}{\hbar}\sqrt{\frac{2m_h^*}{\pi}}$.

AUTHOR INFORMATION

Corresponding Authors

*E-mail: isanchez@isi.edu.

*E-mail: han.wang.4@usc.edu.

ORCID

Xiaodong Yan: 0000-0002-7737-6984

Han Wang: 0000-0001-5121-3362

Ivan Sanchez Esqueda: 0000-0001-6530-8602

Notes

The authors declare no competing financial interest.

ACKNOWLEDGMENTS

The authors acknowledge support from the National Science Foundation (Grant ECCS-1653870) and the Army Research Office (Grant W911NF-18-1-0268).

REFERENCES

(1) Li, L.; Yu, Y.; Ye, G. J.; Ge, Q.; Ou, X.; Wu, H.; Feng, D.; Chen, X. H.; Zhang, Y. Black Phosphorus Field-Effect Transistors. *Nat. Nanotechnol.* **2014**, *9*, 372−377.

(2) Xia, F.; Wang, H.; Jia, Y. Rediscovering Black Phosphorus as an Anisotropic Layered Material for Optoelectronics and Electronics. *Nat. Commun.* **2014**, *5*, 4458.

(3) Xia, F.; Wang, H.; Xiao, D.; Dubey, M.; Ramasubramaniam, A. Two-Dimensional Material Nanophotonics. *Nat. Photonics* **2014**, *8*, 899−907.

(4) Tian, H.; Tice, J.; Fei, R.; Tran, V.; Yan, X.; Yang, L.; Wang, H. Low-Symmetry Two-Dimensional Materials for Electronic and Photonic Applications. *Nano Today* **2016**, *11*, 763−777.

(5) Qiao, J.; Kong, X.; Hu, Z. X.; Yang, F.; Ji, W. High-Mobility Transport Anisotropy and Linear Dichroism in Few-Layer Black Phosphorus. *Nat. Commun.* **2014**, *5*, 1−7.

(6) Liu, H.; Du, Y.; Deng, Y.; Ye, P. D. Semiconducting Black Phosphorus: Synthesis, Transport Properties and Electronic Applications. *Chem. Soc. Rev.* **2015**, *44*, 2732−2743.

(7) Ling, X.; Wang, H.; Huang, S.; Xia, F.; Dresselhaus, M. S. The Renaissance of Black Phosphorus. *Proc. Natl. Acad. Sci. U. S. A.* **2015**, *112*, 4523−4530.

(8) Doganov, R. A.; O'Farrell, E. C. T.; Koenig, S. P.; Yeo, Y.; Ziletti, A.; Carvalho, A.; Campbell, D. K.; Coker, D. F.; Watanabe, K.; Taniguchi, T.; Neto, A. H. C.; Özyilmaz, B. Transport Properties of Pristine Few-Layer Black Phosphorus by van Der Waals Passivation in an Inert Atmosphere. *Nat. Commun.* **2015**, *6*. DOI: 10.1038/ncomms7647

(9) Long, G.; Maryenko, D.; Shen, J.; Xu, S.; Hou, J.; Wu, Z.; Wong, W. K.; Han, T.; Lin, J.; Cai, Y.; Lortz, R.; Wang, N. Achieving Ultrahigh Carrier Mobility in Two-Dimensional Hole Gas of Black Phosphorus. *Nano Lett.* **2016**, *16*, 7768−7773.

(10) Na, J.; Lee, Y. T.; Lim, J. A.; Hwang, D. K.; Kim, G. T.; Choi, W. K.; Song, Y. W. Few-Layer Black Phosphorus Field-Effect Transistors with Reduced Current Fluctuation. *ACS Nano* **2014**, *8*, 11753−11762.

(11) Tian, H.; Deng, B.; Chin, M. L.; Yan, X.; Jiang, H.; Han, S. J.; Sun, V.; Xia, Q.; Dubey, M.; Xia, F.; Wang, H. A Dynamically Reconfigurable Ambipolar Black Phosphorus Memory Device. *ACS Nano* **2016**, *10*, 10428−10435.

(12) Wang, H.; Wang, X.; Xia, F.; Wang, L.; Jiang, H.; Xia, Q.; Chin, M. L.; Dubey, M.; Han, S. Black Phosphorus Radio-Frequency Transistors. *Nano Lett.* **2014**, *14*, 6424−6429.

(13) Li, T.; Zhang, Z.; Li, X.; Huang, M.; Li, S.; Li, S.; Wu, Y. High Field Transport of High Performance Black Phosphorus Transistors. *Appl. Phys. Lett.* **2017**, *110*, 2−5.

(14) Wan, R.; Cao, X.; Guo, J. Simulation of phosphorene Schottky-barrier transistors. *Appl. Phys. Lett.* **2014**, *105*, 163511.

(15) Penumatcha, A. V.; Salazar, R. B.; Appenzeller, J. Analysing Black Phosphorus Transistors Using an Analytic Schottky Barrier MOSFET Model. *Nat. Commun.* **2015**, *6*, 1−8.

(16) Esqueda, I. S.; Tian, H.; Yan, X.; Wang, H. Transport Properties and Device Prospects of Ultrathin Black Phosphorus on Hexagonal Boron Nitride. *IEEE Trans. Electron Devices* **2017**, *64*, 5163−5171.

(17) Das, S.; Chen, H.; Penumatcha, A.; Appenzeller, J. High Performance Multilayer MoS2 Transistors with Scandium Contacts. *Nano Lett.* **2013**, *13*, 100−105.

(18) Lundstrom, M. S. *Fundamentals of Carrier Transport*; Cambridge University Press, 2009.

(19) Lundstrom, M.; Jeong, C. *Near-Equilibrium Transport: Fundamentals and Applications*; World Scientific Publishing Company, 2012.

(20) Esqueda, I. S.; Cress, C. D.; Cao, Y.; Che, Y.; Fritze, M.; Zhou, C. The Impact of Defect Scattering on the Quasi-Ballistic Transport of Nanoscale Conductors. *J. Appl. Phys.* **2015**, *117*, 84319.

(21) Datta, S. *Electronic Transport in Mesoscopic Systems*; Cambridge University Press, 1997.

(22) Esqueda, I.; Cress, C.; Che, Y. Charge Trapping in Aligned Single-Walled Carbon Nanotube Arrays Induced by Ionizing Radiation Exposure. *J. Appl. Phys.* **2014**, *115*, 54506.

(23) Datta, S.. *Quantum Transport: Atom to Transistor*; Cambridge University Press, 2005.

(24) Wong, H.-S. P.; Akinwande, D. *Carbon Nanotube and Graphene Device Physics*; Cambridge University Press, 2011.

(25) Kim, R.; Datta, S.; Lundstrom, M. S. Influence of Dimensionality on Thermoelectric Device Performance. *J. Appl. Phys.* **2009**, *105*, 34506.

(26) Kruglyak, Y. A. A Generalized Landauer-Datta-Lundstrom Electron Transport Model. *Russ. J. Phys. Chem. A* **2014**, *88*, 1826−1836.

(27) Sanchez Esqueda, I.; Cress, C. D. Modeling Radiation-Induced Scattering in Graphene. *IEEE Trans. Nucl. Sci.* **2015**, *62*, 2906−2911.

NOTE ADDED AFTER ASAP PUBLICATION

The version of this paper that was published ASAP December 7, 2018, contained errors in eqs 3 and 4. The corrected version was reposted December 7, 2018.

DOI: 10.1021/acs.nanolett.8b04308
Nano Lett. 2019, 19, 482−487